Title

Quantitative in vivo imaging of neuronal glucose concentrations with a genetically encoded fluorescence lifetime sensor

Journal

Journal of Neuroscience Research, 97(8)

ISSN

0360-4012

Authors

Díaz-García, Carlos Manlio
Lahmann, Carolina
Martínez-François, Juan Ramón
et al.

Publication Date

2019-08-01

DOI

10.1002/jnr.24433

Peer reviewed

10x GENOMICS

The resolution is here

Experience subcellular in situ
from the single cell leader

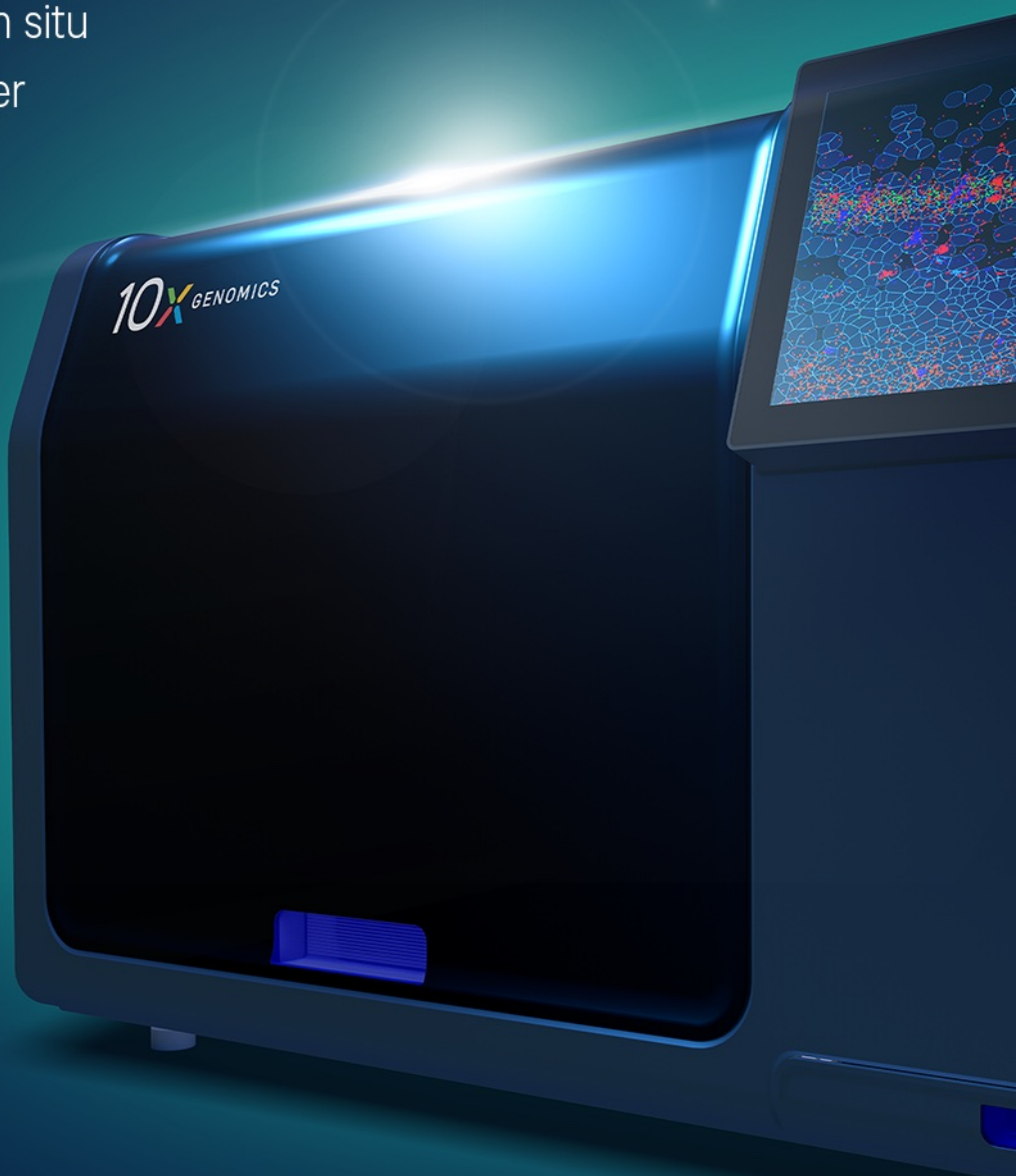

10xgen.com/jointheresolution

Received: 24 January 2019 | Revised: 8 April 2019 | Accepted: 8 April 2019

DOI: 10.1002/jnr.24433

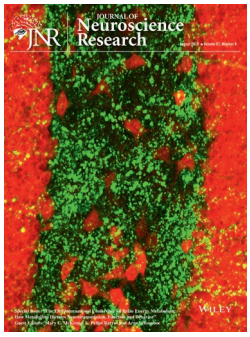

NEUROTECHNIQUE

Quantitative *in vivo* imaging of neuronal glucose concentrations with a genetically encoded fluorescence lifetime sensor

Carlos Manlio Díaz-García[1] | Carolina Lahmann[1] | Juan Ramón Martínez-François[1] | Binsen Li[1] | Dorothy Koveal[1] | Nidhi Nathwani[1] | Mahia Rahman[1] | Jacob P. Keller[2] | Jonathan S. Marvin[2] | Loren L. Looger[2] | Gary Yellen[1]

[1]Department of Neurobiology, Harvard Medical School, Boston, Massachusetts

[2]Janelia Research Campus, Howard Hughes Medical Institute, Ashburn, Virginia

Correspondence
Gary Yellen, Department of Neurobiology, Harvard Medical School, 200 Longwood Avenue, Boston, MA 02115, USA.
Email: gary_yellen@hms.harvard.edu

Funding information
Our work is supported by grants R01 NS102586, R01 GM124038, and DP1 EB016985 (to G.Y.), F32 NS093784 (to C.L.) and F32 NS100331 (to C.M.D.G.) from the NIH/NINDS; and F32 GM123577 (to D.K.) from the NIH/NIGMS

Abstract

Glucose is an essential source of energy for the brain. Recently, the development of genetically encoded fluorescent biosensors has allowed real time visualization of glucose dynamics from individual neurons and astrocytes. A major difficulty for this approach, even for ratiometric sensors, is the lack of a practical method to convert such measurements into actual concentrations in *ex vivo* brain tissue or *in vivo*. Fluorescence lifetime imaging provides a strategy to overcome this. In a previous study, we reported the lifetime glucose sensor iGlucoSnFR-TS (then called SweetieTS) for monitoring changes in neuronal glucose levels in response to stimulation. This genetically encoded sensor was generated by combining the *Thermus thermophilus* glucose-binding protein with a circularly permuted variant of the monomeric fluorescent protein T-Sapphire. Here, we provide more details on iGlucoSnFR-TS design and characterization, as well as pH and temperature sensitivities. For accurate estimation of glucose concentrations, the sensor must be calibrated at the same temperature as the experiments. We find that when the extracellular glucose concentration is in the range 2–10 mM, the intracellular glucose concentration in hippocampal neurons from acute brain slices is ~20% of the nominal external glucose concentration (~0.4–2 mM). We also measured the cytosolic neuronal glucose concentration *in vivo*, finding a range of ~0.7–2.5 mM in cortical neurons from awake mice.

KEYWORDS
energy metabolism, fluorescent biosensor, glucose metabolism

1 | INTRODUCTION

Glucose is an essential energy source in the brain. Brain glucose distribution and utilization has long been studied by several approaches like autoradiography (Sokoloff et al., 1977), magnetic resonance spectroscopy (Ven et al., 2011), and positron emission tomography (Fox, Raichle, Mintun, & Dence, 1988). However, none of these methods provides enough temporal or spatial resolution to reveal glucose dynamics in individual cells in response to naturalistic stimulation (reviewed by Mergenthaler, Lindauer, Dienel, & Meisel, 2013). A newer alternative is the use of fluorescent glucose analogs (Chiquita, Quilichini, Nimchinsky, & Buzsáki, 2010; Lundgaard et al., 2015; Porras, Loaiza, & Barros, 2004). All of these methods measure the behavior of glucose analogs rather than glucose itself, and these

Significance

Glucose fuels energy production in the brain. Thus, monitoring glucose inside cells is important to understand brain metabolism in health and disease. However, knowing the exact glucose concentration at any moment in a particular cell is a challenging task. Here, we characterize a genetically encoded sensor that changes its fluorescence lifetime in response to glucose. Using fluorescence lifetime microscopy, a sensor calibration in permeabilized cells is used to calculate glucose concentrations in individual neurons from brain slices and visual cortex from awake mice. This tool can be applied for quantitative assessment of glucose levels in different cell-types of the brain.

glucose analogs can have different (i) transport or phosphorylation rates, (ii) cellular accumulation, and (iii) competition with glucose for enzymes. These factors complicate data interpretation and direct comparison among studies (Dienel, 2012).

The use of genetically encoded fluorescent biosensors can overcome these limitations. A ratiometric FRET sensor for glucose (Fehr, Lalonde, Ehrhardt, & Frommer, 2004; Takanaga, Chaudhuri, & Frommer, 2008) has been used to detect changes in the intracellular glucose levels from neurons (Piquet et al., 2018) and astrocytes (Bittner et al., 2010, 2011; Ruminot, Schmälzle, Leyton, Barros, & Deitmer, 2019). However, the quantitative assessment of cytosolic glucose concentration in individual cells is still a cumbersome process. *In vitro* calibrations (i.e., using purified protein) may deviate from the expected behavior in cells because of differences in the cellular environment, requiring *in situ* calibration instead (Looger, Lalonde, & Frommer, 2005). Cell permeabilization is often needed to achieve the latter, which might sometimes be suitable in cultured cells, but it is incompatible with more complex preparations like brain slices, or imaging experiments *in vivo*. Use of fluorescence lifetime measurements provides a calibratable optical measurement, independent of the biosensor concentration, to allow quantitative biosensor measurements that can be directly compared between *in vitro* and brain slice or *in vivo* measurements (Yellen & Mongeon, 2015).

We recently used a fluorescence lifetime sensor as a readout of cytosolic glucose levels in resting and stimulated neurons (Díaz-García et al., 2017). This genetically encoded sensor harnesses the glucose-sensing domain from a bacterial protein, coupled to a fluorescent protein; a similar combination (using a different fluorescent protein) was previously engineered into a fluorescence intensity-based sensor (Keller & Looger, 2016; Keller et al., 2019; Marvin, Looger, Lee, & Schreiter, 2018). Here, we present a characterization of the lifetime glucose sensor iGlucoSnFR-TS (previously referred to as SweetieTS), along with an in-cell calibration that is suitable for the experimental data obtained in intact cells. The in-cell calibration was also used to determine the steady-state glucose concentration in individual dentate granule neurons from acute hippocampal slices, and its relationship with glucose concentration in the external solution. We also imaged the sensor in cortical neurons *in vivo* to measure the neuronal glucose concentration in awake mice.

2 | MATERIALS AND METHODS

2.1 | Reagents

All reagents were purchased from Sigma-Aldrich (St. Louis, MO), unless otherwise specified.

2.2 | Animals

Brain slice experiments and *in vivo* imaging were performed using brains of male and female wild-type mice (C57BL/6NCrl; Charles River Laboratories). Animals were housed in a barrier facility in individually ventilated cages with *ad libitum* access to standard chow diet (PicoLab 5053). All experiments were performed in compliance with the NIH Guide for the Care and Use of Laboratory Animals and the Animal Welfare Act. The Harvard Medical Area Standing Committee on Animals approved all procedures involving animals.

2.3 | Sensor design, screening, and characterization

Gene construction, protein purification, and sensor characterization were performed as previously described (Díaz-García et al., 2017; Hung, Albeck, Tantama, & Yellen, 2011).

Protein purification was performed using a Ni Sepharose 6 Fast Flow histidine-tagged protein purification resin (GE Healthcare), following the manufacturer instructions. The resulting eluate was dialyzed in 5 mM of MOPS, 300 mM of NaCl, 10% of glycerol, pH 7.4, and then diluted 1:10 in 100 mM of MOPS, 50 mM of KCl, 5 mM of NaCl, 0.5 mM of $MgCl_2$, and pH 7.4. Excitation maxima were determined from the spectrum scanned between 390 and 500 nm in 5 nm increments, using a Biotek Synergy 4 micro-plate reader (BioTek Instruments, VT). The emission spectrum was also obtained scanning from 435 to 630 nm in 5 nm increments.

Fluorescence lifetime measurements were performed on the same samples using a PR1 plate reader connected to a FLS 980 Spectrometer (Edinburgh Photonics, UK). Illumination was delivered by a pulsed supercontinuum laser Fianium WhiteLase Micro (NKT Photonics, Denmark), filtered by an adjustable bandpass interference filter. The excitation wavelength was set to 435/20 and the emission was collected at 515/20. Several glucose concentrations were tested to obtain dose–response curves in 96-well microplates (0.1, 0.3, 1, 3, and 10 mM). The pH-dependence of the sensor was also determined by adjusting the pH values to 6.5, 6.8, 7.1, 7.4, and 7.7. The experiments with purified protein using 1p-excitation were carried out at room temperature.

To obtain the dose–response curves, the fluorescence lifetime (LT, in ns) data from each experiment was plotted as a function of

glucose concentration ([glucose], in mM), and then fitted to a Hill equation with the form of Equation 1:

$$LT = LT_{min} + \frac{LT_{max} - LT_{min}}{1 + \left(\frac{K_{0.5}}{[glucose]}\right)^{n_H}} \quad (1)$$

where LT_{min} and LT_{max} correspond to lifetimes at the lower and upper asymptotes, respectively, $K_{0.5}$ (in mM) is the midpoint of the curve and n_H is the Hill coefficient, which was fixed to 1.

2.4 | Calculation of fluorescence lifetimes

Reported lifetime values are a standardized "tau8" value defined as:

$$< t_{arrival} >_{0-8ns} = \left(\int_0^{8ns} t \cdot f(t)\, dt \right) / \left(\int_0^{8ns} f(t)\, dt \right) \quad (2)$$

where $f(t)$ is the best-fit two-exponential function to the lifetime decay histogram, with the form:

$$f(t) = A_1 e^{-t/\tau_1} + A_2 e^{-t/\tau_2} \quad (3)$$

Fitting is performed as described in Mongeon, Venkatachalam, and Yellen (2016). Restricting the averaging to the approximate time window of the actual data avoids spurious contributions of the fit function beyond the measurement range (where different two-exponential fits that fit the data equally well may diverge), and thus minimizes differences between individual fits and individual experimental setups.

Calculating the definite integral from Equation 2 for the function defined in Equation 3, results in the "tau8" value of:

$$< t_{arrival} >_{0-8ns} = \frac{e^{-8\left(\frac{1}{\tau_1}+\frac{1}{\tau_2}\right)} \cdot \left(-A_1\tau_1 (8+\tau_1) e^{\frac{8}{\tau_2}} - A_2\tau_2 e^{\frac{8}{\tau_1}} (8+\tau_2) \right) + A_1\tau_1^2 + A_2\tau_2^2}{A_1\tau_1 \left(1 - e^{-\frac{8}{\tau_1}}\right) + A_2\tau_2 \left(1 - e^{-\frac{8}{\tau_2}}\right)}.$$

2.5 | Cell culture and transfection

The cell line HEK293T (ATCC) was grown in Minimum Essential Medium (Gibco or Sigma) containing 5.6 mM of glucose, supplemented with 10% of fetal bovine serum, 100 units/ml of penicillin G, 100 μg/ml of streptomycin, and 2 mM of L-glutamine or Glutamax. Cell cultures were maintained at 37°C in 5% CO_2 and 95% air with humidification.

For transfection, cells were seeded onto protamine-coated coverslips inside 6-well plates until they reached ~50% confluence; they were washed with 2 ml of PBS, and then transfected with 0.4 μg of a plasmid encoding for iGlucoSnFR-TS under the *CAG* promoter, using the Effectene Transfection kit (Qiagen), following the manufacturer instructions.

Intact HEK293T cells were imaged 2–7 days after transfection at ~34°C, using a perfusion rate of 5 ml/min. The bathing solution contained (in mM): 140 of NaCl, 2.5 of KCl, 10 of HEPES, 1 of $MgCl_2$, 2 of $CaCl_2$, and pH 7.4. The glucose concentration was varied during the experiments. In a subset of experiments, cells were incubated at room temperature with 0.5 mM of iodoacetic acid (IAA) for 10 min to inhibit glucose consumption by the enzyme GAPDH, and then transferred to the perfusion chamber.

2.6 | In-cell calibration of the glucose sensor

An in-cell calibration should reflect sensor behavior more accurately, since the cellular environment is preserved. For this, we designed an extracellular solution that mimics the ionic composition of the cytosol, and causes minimal interference with the expected behavior of the sensor. The solution where glucose was applied contained physiological concentrations of K^+, $Na^+$and Cl^- (Alberts et al., 2002), along with gluconate as the major anion (Lutas, Birnbaumer, & Yellen, 2014; Masia, Krause, & Yellen, 2015). Free Mg^{2+} concentration was adjusted within the range of physiological values (Romani & Scarpa, 1992) and free Ca^{2+} was buffered at ~80 nM, which is close to the Ca^{2+} concentration at rest in HEK293 cells (Tong, McCarthy, & MacLennan, 1999), and neurons (Grienberger & Konnerth, 2012). The pH was set to 7.35, since resting pH values from 7.2 to 7.5 have been reported for HEK293 cells (Lang, Wagner, Haddad, Burnekova, & Geibel, 2003; Salvi, Quillan, & Sadée, 2002), and the neuronal cell line Neuro2A (Tantama, Hung, & Yellen, 2011). We also used HEPES, a widely used pH buffer in biological studies with negligible binding to Mg^{2+}, Ca^{2+}, and other metals (Good et al., 1966). The lifetime sensor iGlucoSnFR-TS was calibrated in permeabilized HEK293T cells, using 2 photon-fluorescence lifetime microscopy (2p-FLIM). Cells were incubated at room temperature with 0.5 mM iodoacetic acid (IAA) for 10 min, and then transferred to the perfusion chamber. HEK293T cells were exposed to the following solution (in mM): 140 of K-Gluconate, 10 of NaCl, 10 of HEPES, 1 of EGTA, 1.324 of $MgCl_2$, 0.346 of $CaCl_2$, and pH 7.35 at 34°C. Free concentrations of Mg^{2+} and Ca^{2+} were estimated to be ~1 mM and ~80 nM, respectively, using Chelator (https://web.stanford.edu/~cpatton/CaMgATPEGTA-TS.htm; Schoenmakers, Visser, Flik, & Theuvenet, 1992). After 5–10 min in the solution, the cells were permeabilized with 45 μM β-escin for 2 min, and then washed for 10 min in the solution without the permeabilizing agent.

Similar recordings were performed at 37°C. Temperature was monitored during the experiments using a TC-344C temperature controller (Warner Instruments, Hamden, CT). The thermistor readout was verified and corrected using a thermocouple sensor linked to a BAT-12 thermometer (Sensortek, Clifton, NJ).

For constructing a dose–response curve, each glucose concentration was assessed in a different pool of cells from the same passage/transfection. After changing the glucose concentration, we monitored the fluorescence lifetime of the sensor at intervals ≤ 1 min until it was stable in our sample (usually after 10–20 min). Data for analysis were then collected for 1–5 min at intervals of 10–25 s. Each data point from the dose–response curve corresponds to three independent experiments using different cell passages/transfections.

2.7 | *In vitro* calibration and temperature sensitivity of the glucose sensor

A calibration of purified sensor protein was performed using 2p-FLIM as reported in Díaz-García et al. (2017), following the method described by Mongeon et al. (2016).

The gene encoding iGlucoSnFR-TS was cloned into the pRSetB (Invitrogen) bacterial expression vector, appending an N-terminal 6x His-tag for purification. BL21(DE3) cells were transformed and cultured in 500 ml flasks with 100 ml AIM (Auto Induction Medium; ForMedium, Norfolk, UK) for 24 hr at 37°C with shaking. Protein was purified as described above and dialyzed overnight at 4°C against the K-Gluconate buffer described above. Samples were concentrated using Amicon Ultra centrifugal filters, 10K MWCO (Millipore). The concentration of protein containing mature chromophore was determined by measuring absorbance of the naked chromophore at 447 nm under alkaline denaturing conditions (0.1 M of NaOH, 6 M of guanidine hydrochloride).

Samples were prepared at three different protein concentrations (20, 16, and 9.16 μM; each from a separately purified sample), loaded into a borosilicate glass capillary (Warner Instruments, Hamden, CT) previously sealed by fire-polishing, and imaged at different temperatures in the 2p-microscope. The portion of the pipettes containing the protein was submerged in the same recording chamber used for cultured cells and slices. They were perfused with distilled water at the same flow rate (~5 ml/min), and temperature control was also similar. This data set was used for comparison with the in-cell calibration.

2.8 | Viral vectors

A custom-made adeno-associated viral vector (AAV; Viral Core Facility from Boston Children's Hospital) encoding the glucose sensor iGlucoSnFR-TS (AAV2/8.*CAG*.iGlucoSnFR-TS) was used for expression in the hippocampus and visual cortex.

2.9 | Biosensor expression in hippocampus

For sensor expression in the hippocampus, mice at postnatal day 1 were anesthetized using cryoanesthesia. Following confirmation of anesthesia, pups were injected intracranially with a 2:1 mixture of AAV2/8.*CAG*.iGlucoSnFR-TS (titer = 3.3×10^{14} genome copies/ml) and 0.9% NaCl solution. Pups received two 150 nl viral injections per hemisphere, at the following coordinates with respect to lambda: (i) 0 mm in the anterior-posterior direction, ±1.9 mm in the medial-lateral axis, and −2.0 mm in the dorsal-ventral direction. (ii) 0 mm in the anterior-posterior direction, ±2.0 mm in the medial-lateral axis, and −2.3 mm in the dorsal-ventral direction.

2.10 | Mouse hippocampal slice preparation

Mice between 17 and 24 days old were anesthetized with isoflurane, decapitated, and the brain was placed in ice-cold slicing solution containing (in mM): 87 of NaCl, 2.5 of KCl, 1.25 of NaH_2PO_4, 25 of $NaHCO_3$, 0.25 of $CaCl_2$, 7 of $MgCl_2$, 75 of sucrose, and 25 of D-glucose (335–340 mOsm/kg). Brains were glued by the dorsal side in a chamber containing the same slicing solution and horizontal slices were cut at a thickness of 275 μm using a vibrating slicer (7000smz-2, Campden Instruments, Loughborough, England).

Slices were immediately transferred to a chamber filled with artificial cerebrospinal fluid (ACSF) at 37°C, containing (in mM): 120 of NaCl, 2.5 of KCl, 1 of NaH_2PO_4, 26 of $NaHCO_3$, 2 of $CaCl_2$, 1 of $MgCl_2$, and 10 of D-glucose (~290 mOsm/kg). All solutions were continuously bubbled with a mix of 95% of O_2 and 5% of CO_2, which provides adequate oxygenation and stabilizes the pH around 7.4. Slices were incubated at 37°C for 35 min and then at room temperature for at least 30 min before the experiments, which were executed in the next 4 hr after slicing.

Hippocampal dentate granule neurons were imaged at 25, 50, 100, or 200 μm below the surface of the slice. During the experiments, the slices were perfused with ACSF at a flow rate of 5 ml/min and maintained at 34°C using inline heaters (Warner Instruments, Hamden, CT). To prevent degassing in perfusion line, solutions were preheated at 38°C in a waterless bead bath (Cole-Parmer, Vernon Hills, IL). The extracellular glucose concentration was varied during the course of the experiments.

As in cultured cells, after changing the glucose concentration, we monitored the fluorescence lifetime of the sensor at intervals ≤ 1 min until it was stable in our sample (usually after 10–20 min). Data for analysis were then collected for 1–5 min at intervals of 10–25 s.

2.11 | Two-photon fluorescence lifetime imaging microscopy

Lifetime imaging data were acquired with a modified Thorlabs Bergamo II microscope (Thorlabs Imaging Systems, Sterling, VA), with hybrid photodetectors R11322U-40 (Hamamatsu Photonics, Shizuoka, Japan); the light source was a Chameleon Vision-S tunable Ti-Sapphire mode-locked laser (80 MHz; Coherent, Santa Clara, CA), tuned to 790 nm. The objective lens used for brain slice imaging was an Olympus LUMPLFLN 60x/W (NA 1.0). For *in vivo* imaging, an Olympus XLUMPLFLN 20x/W (NA 1.0) objective was used. Fluorescence emission light was split with an FF562-Di03 dichroic mirror and bandpass filtered for green (FF01-525/50) channel (all filter optics from Semrock, Rochester, NY). The photodetector signals and laser sync signals were pre-amplified and then digitized at 1.25 gigasamples per second using a field-programmable gate array board (PC720 with FMC125 and FMC122 modules, 4DSP, Austin, TX).

Laboratory-built firmware and software performed time-correlated single photon counting to determine the arrival time of each photon relative to the laser pulse; the distribution of these arrival times indicates the fluorescence lifetime (Mongeon et al., 2016; Yellen & Mongeon, 2015). Lifetime histograms were fitted using nonlinear least-squares fitting in MATLAB (Mathworks, Natick, MA), with a two-exponential decay convolved with a Gaussian for the

impulse response function (Yasuda et al., 2006). Microscope control and image acquisition were performed by a modified version of the ScanImage software written in MATLAB (Pologruto, Sabatini, & Svoboda, 2003) (provided by B. Sabatini and modified by G.Y.).

2.12 | Mouse cranial window surgery with AAV injections

Mice (postnatal day 60) were first administered dexamethasone sodium phosphate (30 μL at 4 mg/ml) by an intramuscular injection to the quadriceps 2 hr before surgery. Animals were anesthetized (isoflurane; induction: 2–5%, maintenance: 1.4%), the stereotactic coordinates overlying the primary visual cortex (V1) were marked (0 mm posterior and 2.7 mm lateral to Bregma) and a titanium headplate was attached to the skull using opaque C&B-Metabond (Parkell, Edgewood, NY). A 3 mm round craniotomy with the marked spot at its center was made using a hand-held drill. Following exposure of the brain, the tissue was irrigated with sterile saline and any bleeding stopped using sterile absorbable gelatin sponges.

Four to five injections of a solution containing AAV2/8.*CAG*. iGlucoSnFR-TS (50 nl per injection, 7 min per injection) were made near the center of the craniotomy 200 μm apart from each other at a depth of 200 μm below the dural surface using a beveled glass micropipette attached to a UMP3-1 UltraMicroPump (World Precision Instruments, Sarasota, FL). The surface of the exposed tissue was then covered with a thin layer of Kwik-Sil (to reduce animal movement-induced brain motion that could interfere with imaging; World Precision Instruments, Sarasota, FL) and a glass plug (consisted of a 3 mm diameter coverslip glued to a 5 mm diameter coverslip (both from Warner Instruments, Hamden, CT) using UV-curable optical adhesive (NOA 68; Norland Products, Cranbury, NJ). The glass plug was then cemented to the skull using opaque C&B-Metabond.

After the window implantation surgery, the mice typically woke up after 10 min and were walking around the cage within 15 min. Following 5 days of postoperative recovery, mice were habituated to head-post restraint over a 5-day period. Sessions of head restraint increased in duration over this period from 5 min to 1 hr. Imaging experiments began approximately 10 days post-surgery to allow proper recovery and also steady-state sensor expression.

2.13 | Mouse *in vivo* awake FLIM imaging

In vivo imaging experiments were conducted with awake, unanesthetized mice, as it has been previously demonstrated that anesthesia increases the apparent oxygen concentration of intact brain (Lyons, Parpaleix, Roche, & Charpak, 2016). During imaging, mice were placed on a 6-inch foam ball that could spin noiselessly on ball bearings. Their head was restrained using the previously implanted headplate.

Imaging sessions were 1–2 hr in duration. Viral expression of iGlucoSnFR-TS permitted recording from different neurons in the same mice on different days (Andermann, Kerlin, & Reid, 2010; O'Connor, Peron, Huber, & Svoboda, 2010). When imaging from the same cortical region on multiple days, previously imaged neurons were re-identified using the pattern of the surface vasculature as guidance, and then an adjacent volume was selected to ensure that all neurons in the sample were unique.

2.14 | Lifetime imaging quantification

Image analysis was performed using MATLAB software developed in our laboratory. Regions of interest (ROIs) were defined around individual cells, and photon statistics were calculated for all pixels within the ROI. Typical ROIs encompassed 100–900 image pixels, in images of 128 × 128 (in cells and brain slices) or 256 × 256 pixels (*in vivo*) acquired at a scanning rate of 2 ms per line. Data points of lifetimes are for the mean value of 20 sequentially acquired frames.

Since the *in vivo* recordings were performed with slightly different settings for the lifetime measurements, the data were corrected to match the conditions of the in-cell calibration. Briefly, iGlucoSnFR-TS lifetime was measured in both settings using different glucose concentrations and a linear regression was obtained. The raw *in vivo* data were interpolated in the resulting fit and the corrected values used for estimating the intracellular glucose concentration.

2.15 | Statistical analysis

Curve fitting and statistical analysis were performed using GraphPad Prism v7.05 (GraphPad Software, San Diego, CA). Data were tested with a D'Agostino and Pearson normality test. Since at least one experimental group in each condition significantly deviated from a Gaussian distribution, we chose non-parametric tests for statistical analysis. We selected a Mann–Whitney test for unpaired comparisons between two groups; whereas a Kruskal–Wallis test with a Dunn's post hoc test was used for multiple comparisons. For comparing paired data in more than two conditions, we selected a Friedman test with a Dunn's post hoc test for multiple comparisons. No power analysis was conducted a priori. Graphics were constructed using Origin 2015 (OriginLab, Northampton, MA). Descriptive statistics are specified in the figure legends.

3 | RESULTS

To construct a fluorescence lifetime-based glucose sensor, we started with the fluorescence intensity-based sensor iGlucoSnFR, which consists of circularly permuted GFP (cpGFP) inserted between residues 326 and 327 of *Thermus thermophilus* glucose binding protein (TtGBP, Cuneo, Changela, Warren, Beese, & Hellinga, 2006); TtGBP-to-cpGFP and cpGFP-to-TtGBP linkers were optimized, and two binding-site residues, His66 and His348, were mutated to alanine to reduce glucose-binding affinity to 2.3 mM (Keller & Looger, 2016; Keller et al., 2019; Marvin et al., 2018). We replaced cpGFP with a circularly permuted version of the GFP mutant T-Sapphire (Zapata-Hommer & Griesbeck, 2003), and then screened a library of mutants of both linkers, and screened for the glucose-dependent

change in T-Sapphire fluorescence lifetime, binding affinity, and pH dependence. Based on its high fluorescence lifetime change and low pH sensitivity, we selected a mutant with the original TtGBP-to-cpGFP linker changed from Pro-Ala to Pro-Asp, and the original cpGBP-to-TtGBP linker changed from Asn-Pro to Glu-Pro (Figure 1a). This sensor was named iGlucoSnFR-TS, adding the notation TS for the fluorophore T-Sapphire. The excitation spectrum shows a principal maximum around 400 nm and a local secondary maximum near 480 nm, whereas the emission spectrum shows a single prominent maximum at 510 nm (Figure 1b). When excited with a wavelength near 400 nm, the fluorescent lifetime of the sensor varied systematically between 1.6 and 1.9 ns in response to changes in the glucose concentration from 0.1 to 10 mM (Figure 1c).

To assess the pH sensitivity of iGlucoSnFR-TS, we measured dose–response curves of iGlucoSnFR-TS (as purified protein) at different pH values in the relevant physiologic range of 6.5–7.7. At pH values of 7.1 and 7.4, there was little noticeable difference in fluorescence lifetime due to pH, in the [glucose] range from 0.3 to 10 mM (Figure 1c). There was lifetime variation with pH at lower [glucose] of 0.1 mM or at more extremes of pH (Figure 1c). The lifetime values and the dynamic range observed in these experiments, performed at room temperature using 1p-excitation, suggested that iGlucoSnFR-TS could be suitable for imaging biological samples using digital 2p-FLIM.

Because the calibration based on purified protein may not match the range of sensor lifetime in cells, we performed an in-cell

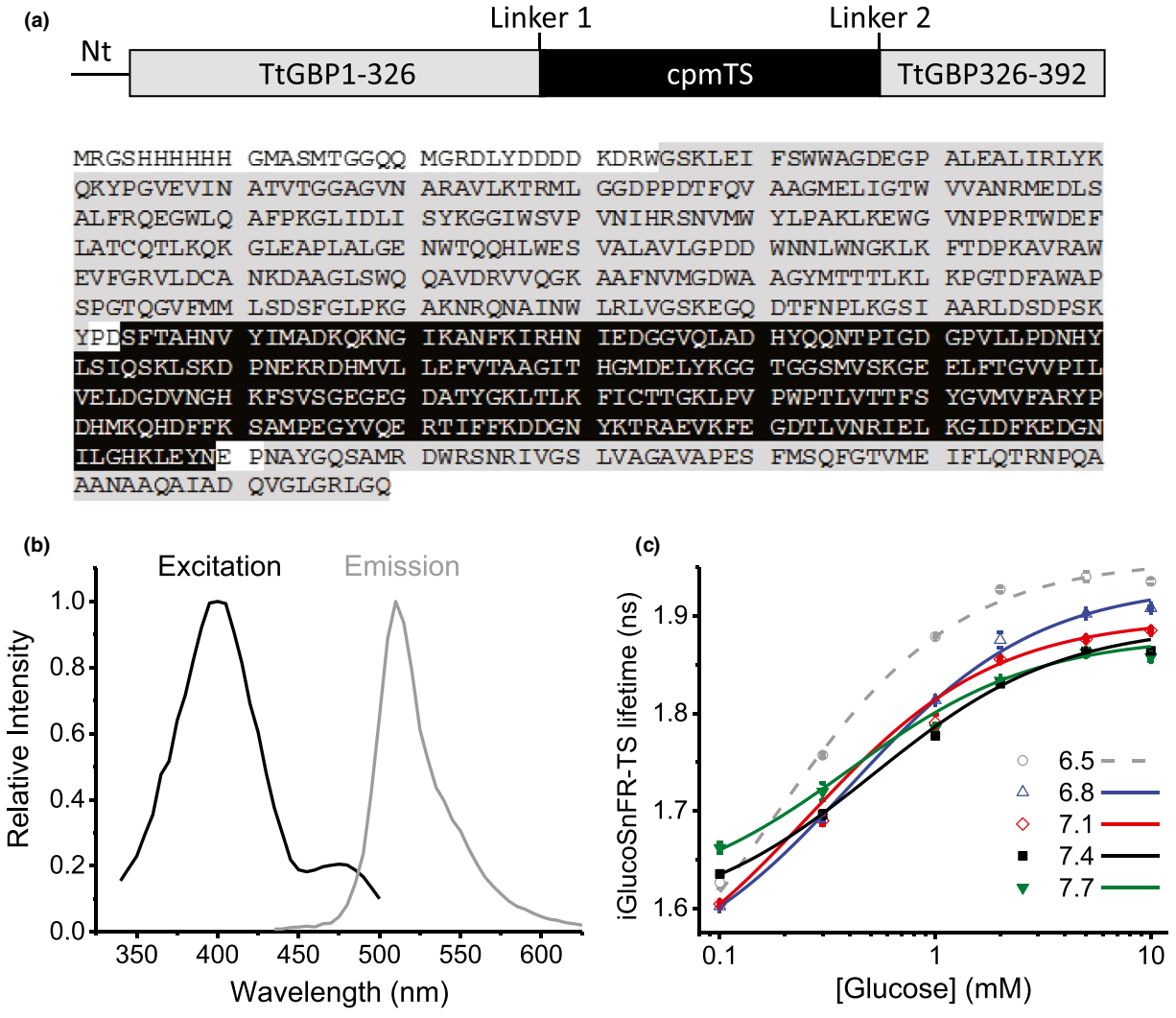

FIGURE 1 Sensor design and characterization. (a) *Top*, schematic representation of the glucose sensor. Abbreviations indicate the N-terminal pRSET affinity tag sequence (Nt), the glucose-binding protein (TtGBP) and the circularly permuted T-Sapphire (cpmTS). *Bottom*, the full sequence of the sensor as reported in Díaz-García et al. (2017), highlighting each domain with the same color code from the schematic representation. (b) Excitation and emission spectra of the purified sensor protein. (c) Dose–response curves at different pH values. Data points and whiskers represent the mean and the range of duplicate measurements, respectively. The curves represent the best fit to a Hill equation (see Equation 1 in Methods). Experiments were performed at room temperature of approximately 22°C

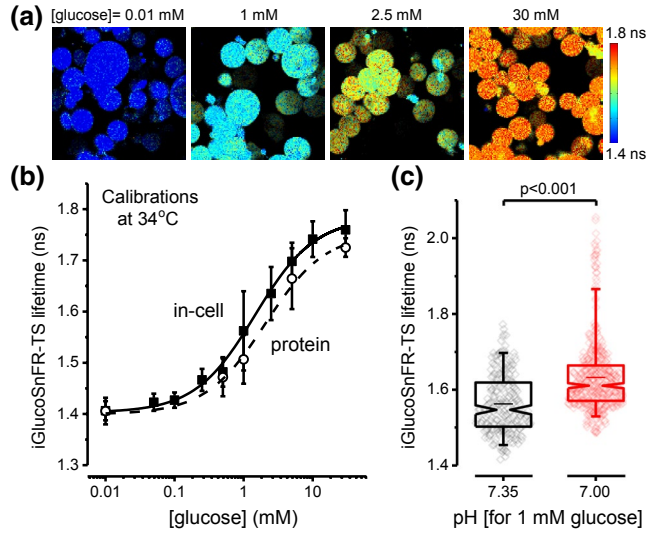

FIGURE 2 Calibration of the lifetime sensor iGlucoSnFR-TS. (a) Representative images of IAA-treated, permeabilized HEK293T cells visualized by 2p-FLIM. The cells were incubated at different glucose concentrations after permeabilizing with β-escin. Cells exposed to higher glucose concentrations in the bath perfusion exhibited higher fluorescence lifetimes of the sensor. Note that permeabilization with β-escin caused HEK293T cells to adopt a round shape. (b) Dose–response curve obtained in permeabilized HEK293T cells, at 34°C. Points represent the mean ± *SD* of 133–258 cells from three independent experiments (N = 3, each for a particular passage/transfection). The solid line corresponds to the curve obtained using averaged parameters from three different experiments (see Table 1). The dashed line represents the *in vitro* calibration of the purified sensor, performed under similar conditions. Points represent the mean ± *SD* of three independent experiments (N = 3, each for a particular protein preparation). (c) Low pH increases the lifetime of the sensor in permeabilized cells at 34°C. The cells were bathed with a solution containing 1 mM glucose, with the pH adjusted to 7.35 (N_{cells} = 238, imaged in different fields from three coverslips, each from a different passage/transfection) or 7.00 (N_{cells} = 471, imaged in different fields from three different coverslips, from the same passage/transfection). Box plots indicate the median and middle half of the data, with whiskers spanning the 5–95 percentiles of the population. The notch represents the 95% confidence interval around the median, and the horizontal line indicates the mean. The raw data is overlapped to the box plots. Significance levels were obtained using an unpaired non-parametric Mann–Whitney test

calibration to preserve the natural environment where the sensor is expressed, using β-escin to permeabilize the cells. After permeabilization, HEK293T cells adopted a round, swollen shape (Figure 2a), potentially diluting the sensor inside the cells. However, this did not hinder the detection of sensor signals: increases in laser power achieved photon counts close to the initial fluorescence intensity, and sensor lifetime is independent of concentration.

When we calibrated iGlucoSnFR-TS in permeabilized HEK293T cells for a range of [glucose] from 0.01 to 30 mM, the maximum fluorescence lifetime change of the sensor was ~0.38 ns (Figure 2b). This in-cell calibration slightly deviated from the *in vitro* calibration of purified iGlucoSnFR-TS, also performed using 2p-FLIM and at similar near-physiologic temperature (Figure 2b). Although the total change in lifetime was similar between conditions (~0.36 ns in protein), the absolute values were slightly higher when the sensor signal was measured in a cellular environment. Additionally, the apparent K_d decreased by 1.4-fold, indicating a higher apparent affinity when iGlucoSnFR-TS is in a cellular environment (Figure 2b and Table 1).

We also explored the pH dependence of iGlucoSnFR-TS, expressed in HEK293T cells. Permeabilized cells, perfused with a solution containing 1 mM glucose and pH 7.00, exhibited fluorescence lifetime that was higher by ~0.07 ns compared to cells imaged at pH 7.35 (Figure 2c). This would correspond to a gain of 0.02 ns per decrease in 0.1 pH unit, leading to a ~24% overestimation of the $[glucose]_i$ per 0.1 pH unit of acidification.

The fluorescence lifetime of the sensor in intact (i.e., non-permeabilized) cultured HEK293T cells changed in response to changes in the extracellular glucose concentration in the range 2–10 mM (Figure 3a,b). Lifetime values for iGlucoSnFR-TS were more dispersed in intact HEK293T compared to those in permeabilized cells. Variability in the distributions may arise from different rates of transport/consumption of glucose in these cells, or for indirect reasons like differences in the population of cytosolic pH values, which may contribute to the apparent higher variation by affecting the lifetime of the sensor.

We applied the in-cell calibration to calculate the intracellular glucose concentration in the intact HEK293T cells. In all the experimental conditions tested, medians of the calculated intracellular glucose concentrations were lower than the glucose concentration in the bath, similar to observations in other cultured cells imaged with different fluorescent biosensors (Kovacic et al., 2011; Zhang et al.,

TABLE 1 Parameters from in-cell and *in vitro* calibrations, using 2p-excitation

Calibration	Temp. (°C)	LT_{min} ± *SD* (ns)	LT_{max} ± *SD* (ns)	$K_{0.5}$ ± *SD* (mM)	n_H
In-cell	34	1.403 ± 0.009	1.784 ± 0.012	1.46 ± 0.50	1
	37	1.370 ± 0.010	1.752 ± 0.020	1.79 ± 0.32	1
In vitro	34	1.399 ± 0.023	1.754 ± 0.035	2.07 ± 0.78	1
	37	1.354 ± 0.041	1.697 ± 0.040	2.17 ± 0.60	1

The Hill coefficient (n_H) was set to 1 in the fits. Values for the other parameters are expressed as the mean ± *SD* of three independent dose–response curves.

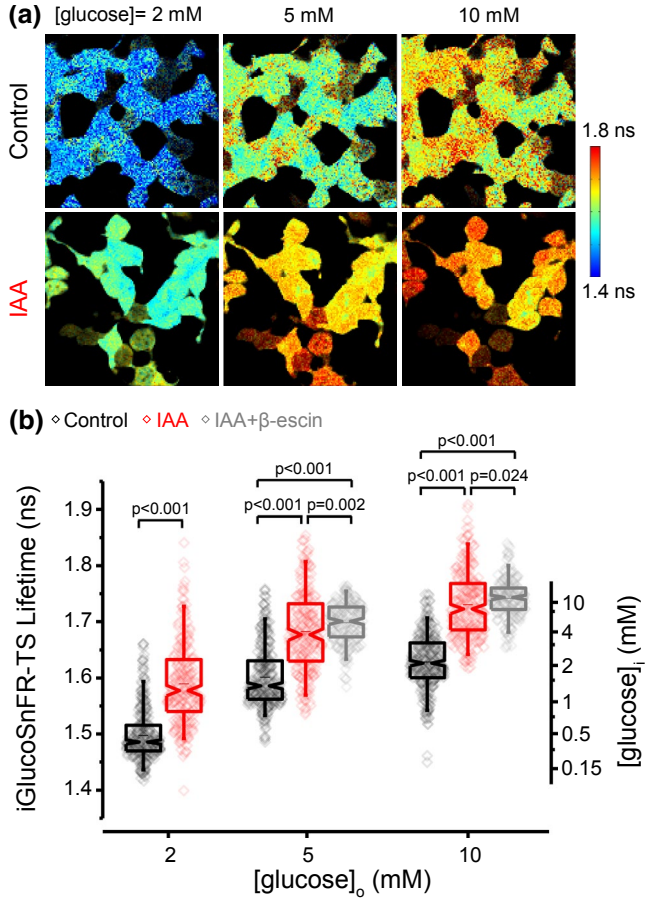

FIGURE 3 Determination of the intracellular glucose concentration in HEK293T cells. (a) *Top:* Representative images of non-permeabilized cells exhibit the typical flat, adherent appearance of HEK293T cells. The fluorescence lifetime of iGlucoSnFR-TS was sensitive to changes in the extracellular glucose concentration. *Bottom:* Cells exhibit higher lifetime values after glycolytic inhibition with 0.5 mM of IAA for 10 min at room temperature. (b) Glucose sensor measurements on intact HEK293T cells at 34°C, as a function of $[glucose]_o$. Box plots indicate the median and middle half of the data, with whiskers spanning the 5–95 percentiles of the population. The horizontal line indicates the mean. The notch represents the 95% confidence interval around the median, and the horizontal line indicates the mean. The raw data is overlapped to the box plots. The right-hand axis indicates the calculated intracellular glucose concentration from the permeabilized-cell calibration. Data were collected from 374 cells in two independent experiments (each for a particular passage/transfection) for the control condition (black box plot). The data set for the treatment with IAA (depicted in red) comprises 248 cells imaged in several fields from three coverslips of two independent passages/transfections. Data from cells treated with IAA, and permeabilized with β-escin (shown in gray), are included for the conditions of 5 and 10 mM glucose (N_{cells} = 219 and 212, respectively, imaged in different fields from three coverslips, each from a different passage/transfection). Experiments were performed at 34°C. For comparisons in the groups at 2 mM glucose, an unpaired non-parametric Mann–Whitney test was used. Significance levels for multiple comparisons at 5 and 10 mM glucose were obtained using an unpaired non-parametric Kruskal–Wallis test with a Dunn's post hoc test

2014). This could reflect an inability of glucose transport to keep up with glucose consumption. Pre-incubating the cells with iodoacetic acid (IAA), to inhibit the glycolytic enzyme GAPDH, and thus reduce glucose consumption increased the reported intracellular [glucose] by more than a 2.5-fold in all the conditions tested (Figure 3b). Even this manipulation, however, did not achieve complete equilibration between the intracellular and the extracellular glucose concentrations as observed by the lower lifetimes compared to IAA-treated, permeabilized cells (Figure 3b).

We then characterized iGlucoSnFR-TS reports of intracellular [glucose] in response to altered extracellular glucose in acute mouse hippocampal brain slices. Hippocampal dentate granule neurons from brain slices also exhibited proportional changes in iGlucoSnFR-TS lifetime in response to variations in the external glucose concentration (Figure 4a,b). Lifetime values were below the values expected for full equilibration of glucose concentrations between the intracellular space and the bath (Figure 4b), indicating that average intracellular glucose concentrations were about 20% of the extracellular levels.

The variability of the measurements was greater when imaging at a relatively shallow depth of 25 µm, rather than 50–200 µm,

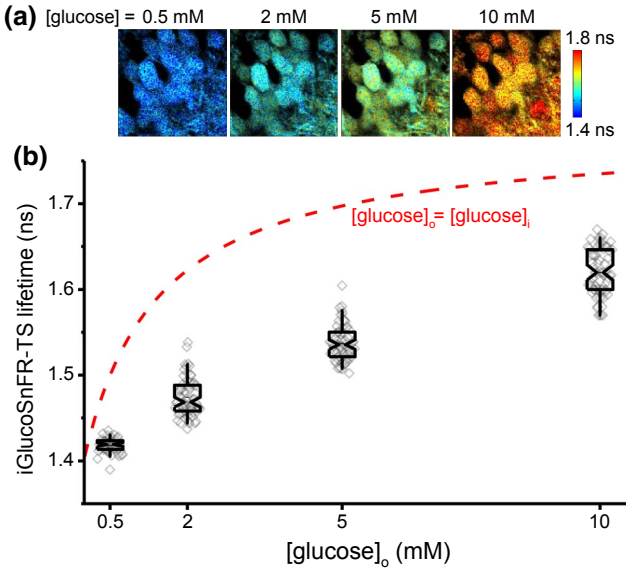

FIGURE 4 Neuronal glucose concentrations in mouse brain slices. (a) Representative images of dentate granule neurons located 50 µm deep into a hippocampal slice, exposed to different glucose concentrations in ACSF. (b) Box plots indicate the median and middle half of the data, with whiskers spanning the 5–95 percentiles of the population. The notch represents the 95% confidence interval around the median, and the horizontal line indicates the mean. The raw data is overlapped to the box plots ($N_{neurons}$ = 51, N_{slices} = 4 and N_{mice} = 2 for $[glucose]_o$ = 0.5 mM; $N_{neurons}$ = 69, N_{slices} = 6 and N_{mice} = 3 for 2, 5 and 10 mM glucose in the ACSF). Experiments were performed at 34°C. The red dashed line represents the expected sensor lifetime when the intracellular glucose concentration is equilibrated with the nominal glucose concentration in the bath (predicted from the in-cell calibration in Figure 2)

below the slice surface (Supplementary Figure 1). It is likely that this is a result from more damaged cells because of the proximity to the blade during the slicing process, hyperoxygenation from being more exposed to the bathing solution, or a combination of both. Neuronal health can be assessed by monitoring Ca^{2+} levels at rest, co-expressing a genetically encoded calcium sensor of a different color. However, quantitative measurements of glucose concentration would require correction for cross-contamination between sensors (Díaz-García et al., 2017), which may add some degree of uncertainty and variability to the measurements.

We studied the effect of glycolytic inhibition on the neuronal glucose concentration in brain slices, using IAA as previously reported (Díaz-García et al., 2017). Lactate was provided as an alternative fuel for the cells to attenuate the effects on cell health of glycolytic inhibition. In order to prevent further damage in the slices, IAA was applied at lower temperatures and a cocktail of synaptic blockers was also included in the bath solution. Dentate granule neurons exhibited a 20 ± 10% increase in the intracellular glucose concentration after IAA-treatment, smaller than the increase seen with IAA in the HEK293T cells, and still below the 10 mM glucose in the superfusion solution (Figure 5).

Before assessing glucose concentrations *in vivo*, we determined the temperature sensitivity of iGlucoSnFR-TS, considering that body temperature in mice is ~37°C (Habicht, 1981). The fluorescence lifetime of the sensor was inversely correlated with temperature (Figure 6a). The temperature dependence of the sensor was characterized by the slope of the linear regression of the lifetime dependence on temperature (Figure 6b). A rate of change in lifetime of −0.019 ns/°C for iGlucoSnFR-TS is equivalent to apparent changes in the glucose concentration of approximately −20%/°C near [glucose] = 1 mM. The latter implies that applying a calibration curve obtained at ~34°C to data collected in a system at 37°C (e.g., *in vivo*), would underestimate glucose concentrations around 1 mM in more than 50%.

To overcome this drawback of the sensor, we obtained the calibration curve in permeabilized HEK293T cells at 37°C (Figure 6c). As expected, the lifetime values were slightly smaller than the calibration curve at 34°C, although the dynamic range was the same (~0.38 ns). The trend of even smaller lifetime values in the calibration using purified sensor at 37°C was also similar to 34°C. However, the $K_{0.5}$ values moved to the right at 37°C, indicating a lower apparent affinity of iGlucoSnFR-TS for glucose at higher temperatures (Table 1).

Finally, we measured iGlucoSnFR-TS fluorescence lifetime in cortical layer 2/3 neurons of awake mice. The lifetime values measured *in vivo* fell within the dynamic range of the in-cell calibration of iGlucoSnFR-TS at 37°C, showing a pattern similar to those of the dentate granule neurons in acute hippocampal brain slices. Furthermore, the *in vivo* estimated intracellular glucose concentrations matched those seen in brain slices perfused with 5–10 mM glucose in the external solution, spanning a range of 0.7–2.5 mM (Figure 6d).

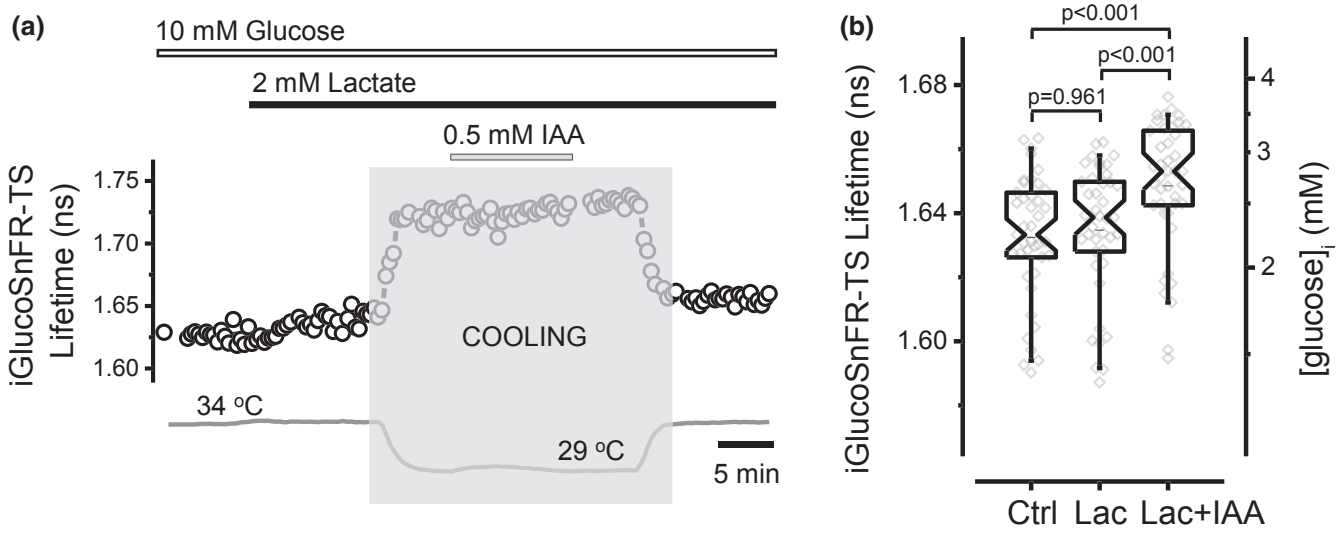

FIGURE 5 Glycolytic inhibition increases neuronal glucose concentrations in acute mouse brain slices. (a) Representative trace of iGlucoSnFR-TS lifetime in an experiment designed to assess intracellular glucose concentration in a dentate granule neuron upon glycolysis inhibition. The bars indicate the times of application of fuels (10 mM glucose and 2 mM lactate), as well as IAA (0.5 mM), which inhibits glycolysis irreversibly. The temperature was lowered (shaded zone) to minimize cell damage during IAA application (The change in the fluorescence lifetime after cooling and heating reflects the temperature sensitivity of the sensor, see Figure 6). To minimize the effects of dysregulated synaptic activity, a cocktail of synaptic blockers was used: 5 μM NBQX, 25 μM D-AP5, and 100 μM Picrotoxin to inhibit AMPA, NMDA, and $GABA_A$ ionotropic receptors, respectively. (b) Addition of lactate (Lac) to the ACSF did not affect the $[glucose]_i$, but subsequent glycolytic inhibition with IAA (Lac + IAA) increased the fluorescence lifetime of the sensor, indicating an elevation in $[glucose]_i$. Box plots indicate the median and middle half of the data, with whiskers spanning the 5–95 percentiles of the population. The notch represents the 95% confidence interval around the median, and the horizontal line indicates the mean. The raw data is overlapped to the box plots ($N_{neurons}$ = 41, N_{slices} = 5 and N_{mice} = 3). Significance levels were obtained using a paired non-parametric Friedman test with a Dunn's post hoc test for multiple comparisons. One outlier data point was omitted because it was > 5 *SD* below the mean

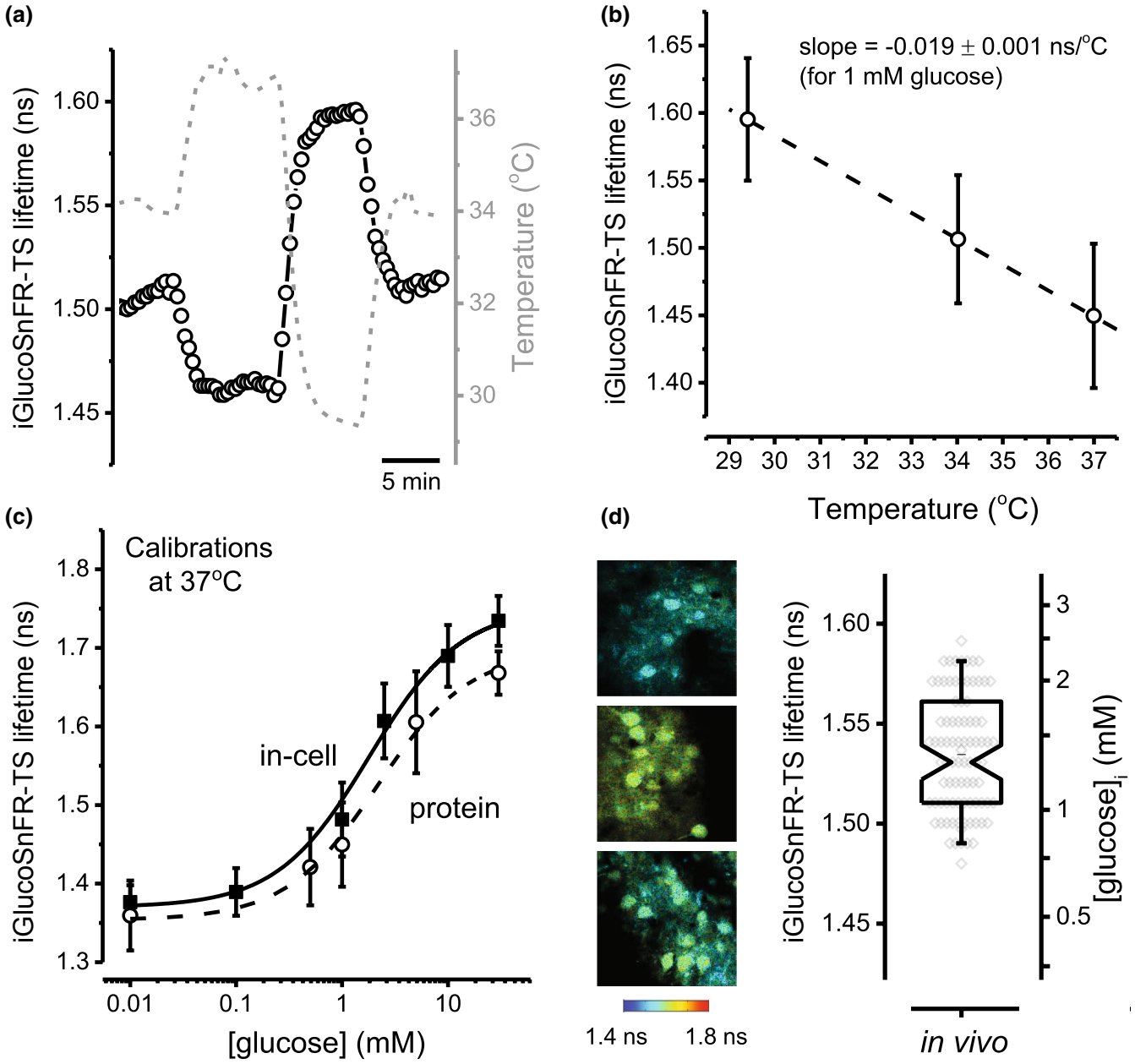

FIGURE 6 Temperature sensitivity of iGlucoSnFR-TS and quantitative *in vivo* imaging of neuronal glucose concentrations. (a) Representative trace of iGlucoSnFR-TS lifetime of a protein sample (black open circles, scale on left axis), imaged in a glass pipette loaded with a solution containing 1 mM glucose. The temperature of the bath (gray dashed line, scale on right axis) was varied over time and the fluorescence lifetime of iGlucoSnFR-TS followed with changes in the opposite direction. (b) A linear regression performed on lifetime values at three different temperatures (29.41 ± 0.04, 34.02 ± 0.05, and 37.0 ± 0.1°C), shows a negative relationship between iGlucoSnFR-TS lifetime and temperature of −0.019 ns per degree Celsius (slope of the curve). Data points represent the mean ± *SD* of three independent experiments. The dashed line was constructed with the average parameters of individual linear regressions from each experiment. (c) Dose–response curve in permeabilized HEK293T cells at 37°C. Solid symbols represent the mean ± *SD* of 82–146 cells from three independent experiments (*N* = 3, each for a particular passage/transfection). The solid line corresponds to the curve obtained using averaged parameters from three different experiments (see Table 1). The dashed line represents the *in vitro* calibration of the purified sensor, performed under similar conditions. Open symbols represent the mean ± *SD* of three independent experiments (*N* = 3, each for a particular protein preparation). (d) *Left*, representative images of neurons from the visual cortex of awake mice expressing the sensor iGlucoSnFR-TS. *Right*, summary of lifetime measurements in V1 neurons (left axis), converted to glucose concentrations (right axis) using the in-cell calibration obtained at 37°C. The calculated *in vivo* $[glucose]_i$ in V1 neurons was 1.41 ± 0.45 mM (mean ± *SD*; $N_{neurons}$ = 87, N_{mice} = 5). The box plot represents the median and middle half of the data, with whiskers spanning the 5–95 percentiles of the population. The notch represents the 95% confidence interval around the median, and the horizontal line indicates the mean. The raw data are overlapped to the box plot

4 | DISCUSSION

iGlucoSnFR-TS is a genetically encoded sensor that changes its fluorescence lifetime in response to glucose concentration. The fluorescence lifetime was minimally affected by pH in the range of 7.1–7.4, which indicates that it is suitable for the measurement of cytosolic glucose concentrations. In principle, the calibration of purified iGlucoSnFR-TS fluorescence lifetimes should be appropriate for calculating the glucose concentration in cells recorded under similar imaging conditions. However, *in vitro* calibrations may not fully recapitulate the sensor behavior in cells, considering that its signal can be affected by the cellular environment (Dittmer, Miranda, Gorski, & Palmer, 2009). For example, genetically encoded, engineered protein sensors can be sensitive to molecular crowding (Dittmer et al., 2009; Morikawa et al., 2016), which is a major distinction between the purified protein and the in-cell calibrations.

We note that even the in-cell calibration may not provide a completely accurate reference for the intact cell measurements. The cell swelling observed with permeabilization would tend to reduce the molecular crowding effect of cytoplasm by dilution. However, this could suggest that a more proper calibration might deviate even further away from the purified protein calibration, in which case the inferred glucose concentrations in neurons would be even more depressed compared to the [glucose] in the bathing solution.

Even though the *in vitro* calibration did not deviate dramatically from the in-cell calibration when the same solutions were used under a strict control of the bath temperature, values from the *in vitro* calibration clearly overestimate the glucose concentration in permeabilized HEK293T cells, where the intracellular and the extracellular glucose concentrations should be equilibrated. Thus, the more comparable in-cell calibrations were used for estimating the intracellular glucose concentration in non-permeabilized HEK293T cells, and also in individual neurons from acute brain slices or the brains of awake mice.

4.1 | Measurement of intracellular [glucose] using iGlucoSnFR-TS in cultured cells and acute brain slices

We observed that the average iGlucoSnFR-TS fluorescence lifetime in cultured HEK293T cells or in dentate granule neurons in acute hippocampal slices robustly responded to changes in the external [glucose], indicating that glucose can rapidly achieve a steady state between the extracellular and the intracellular compartments. However, we observed that the intracellular [glucose] reported by the iGlucoSnFR-TS fluorescence lifetime was consistently lower than the predicted value for full equilibration of intracellular [glucose] with glucose in the bath (Figures 3 and 4). This is similar to observations in cultured cells imaged with different fluorescent biosensors (Kovacic et al., 2011; Zhang et al., 2014). Indeed, metabolite levels do not necessarily match with metabolic fluxes since the concentration of a particular molecule will depend on the balance between consumption/production and transport (Jang, Chen, & Rabinowitz, 2018). Therefore, this difference between external and internal [glucose] might be due to glucose transport being insufficient to keep up with glycolytic glucose consumption. To examine this, we inhibited glycolytic glucose consumption in HEK293T cells or dentate granule neurons with IAA, and observed an increase in intracellular [glucose] in both preparations (Figures 3 and 5). A crucial difference between the two preparations, however, is that in HEK293T cells, partial inhibition of glucose consumption produced > 2.5-fold increase in cytosolic [glucose] to values approaching extracellular [glucose], while in acute slices, partial inhibition increased cytosolic [glucose] by only ~20%.

These observations suggest that the rate of glucose consumption exceeds its transport capacity in cultured, highly glycolytic, HEK393T cells. However, in non-stimulated brain slices, this idea seemed like an unlikely explanation. Many studies support the idea of a higher transport capacity versus glucose consumption in the brain (Cremer, Seville, & Cunningham, 1988; Duarte & Gruetter, 2012; Duarte, Morgenthaler, Lei, Poitry-Yamate, & Gruetter, 2009), and this marked imbalance should be even more pronounced in brain slices, which exhibit a lower glucose consumption rate due to deafferentation (Dienel, 2013). Therefore, the low levels of intracellular [glucose] in dentate granule neurons in hippocampal slices seem more likely due to diffusion barriers between the bathing solution and the slice. In fact, the small intracellular [glucose] increase upon IAA treatment could be due not only to decreased glucose consumption in each neuron, but also to the aggregate effect on the interstitial [glucose] from decreasing consumption by all cells in the slice. On the other hand, we cannot rule out a larger contribution of cellular glucose consumption on intracellular [glucose], as it is possible that the IAA treatment in slices was less effective in inhibiting glucose consumption; it would be hard to assess the effect of stronger inhibition, as slice health is rapidly compromised with IAA treatment (Díaz-García et al., 2017).

If consumption across the slice gradually reduces the interstitial glucose concentration, deeper neurons could also be restricted in the available glucose, compared to shallower areas. Surprisingly, our observations showed the opposite. We observed that untreated neurons closer to the slice surface showed lower [glucose] than those deeper in the slice.[1] Neurons located near the surface could be more damaged and maybe more avid for glucose, but at the same time, they could be more exposed to glucose and O_2 from the superfusion solution. Indeed, neurons are deprived of O_2 deeper in the slice (Engl, Jolivet, Hall, & Attwell, 2017; Ivanov & Zilberter, 2011), which may force them to rely on glycolysis. To fully address this unexpected outcome we would need to measure the interstitial glucose concentration, but performing this measurement in the vicinity of single cells is challenging. In principle, this could be achieved in the

[1] Because the iGlucoSnFR-TS sensor is quite sensitive to temperature, we must also consider the possibility that the temperature was slightly lower deeper in the slice (and farther from the warmed superfusion solution), producing higher lifetime values.

future by targeting iGlucoSnFR-TS to the extracellular side of the plasma membrane.

4.2 | Measurement of intracellular [glucose] using iGlucoSnFR-TS *in vivo*

In the visual cortex of awake mice, the fluorescence-lifetime sensor iGlucoSnFR-TS allowed us to estimate the intracellular [glucose] at 0.7–2.5 mM for individual neurons. Our estimated intracellular [glucose] falls in the lower range of reported tissue values of 0.1–6 mM, which include some contribution from blood and extracellular/cerebrospinal fluid (Choi, Lee, Kim, & Gruetter, 2001; Cremer et al., 1988; Dienel, Cruz, Mori, Holden, & Sokoloff, 1991). Our estimated intracellular [glucose] is also close to values reported for extracellular/cerebrospinal fluid (Leen, Willemsen, Wevers, & Verbeek, 2012; Silver & Erecińska, 1994). Based on calculations obtained from brains of anesthetized rats (Lewis, Ljunggren, Norberg, & Siesjö, 1974), an average intracellular glucose concentration in the brain of ~1.4 mM (similar to our data), would correspond to glucose concentrations in cerebrospinal fluid and blood of ~2 and 4 mM, respectively. This would agree with extracellular and intracellular compartments close to equilibrium, as it has been previously proposed (Pfeuffer, Tkáč, & Gruetter, 2000).

4.3 | iGlucoSnFR-TS is a valuable tool to investigate brain metabolism

Glucose concentration in other cell types in the brain could be measured by expressing iGlucoSnFR-TS with the proper combination of AAV serotype and promoter. Expressing a FRET sensor in cultured astrocytes, the intracellular [glucose] in these cells has been estimated as ~0.4 mM (Prebil, Vardjan, Jensen, Zorec, & Kreft, 2011). Similar results have been obtained for cultured astrocytes and neurons, although differences in their glycolytic rates were not evident (Bittner et al., 2010).

Ideally, glucose handling must be assessed *in vivo*, or at least in more physiologic conditions like in acute brain slices. Determining how glucose levels and dynamics behave in these cells will contribute to solving the longstanding debate on the astrocyte-neuron lactate shuttle (Bak & Walls, 2018; Barros & Weber, 2018; Magistretti, Sorg, Yu, Martin, & Pellerin, 1993), which claims that glucose is preferentially consumed by astrocytes, which in turn provide lactate to neurons. Taking together these scenarios, we anticipate that iGlucoSnFR-TS will be a valuable tool to address fundamental questions about brain metabolism.

In summary, the use of the fluorescence-lifetime sensor iGlucoSnFR-TS allows the assessment of glucose concentrations deep within *ex vivo* or *in vivo* tissue while achieving high spatial resolution (here reported at the cellular level). It is advisable to perform both in-cell and purified-protein calibrations to determine how much the sensor response depends on the cellular environment, and it is necessary to use a calibration matched to the experimental temperature. Using the in-cell calibration, we calculated glucose concentration from individual cortical neurons *in vivo* that agree with reported values for brain tissue.

DECLARATION OF TRANSPARENCY

The authors, reviewers, and editors affirm that in accordance to the policies set by the Journal of Neuroscience Research, this manuscript presents an accurate and transparent account of the study being reported and that all critical details describing the methods and results are present.

ACKNOWLEDGMENTS

We are grateful to the reviewers for improving our manuscript with their comments and suggestions. We also thank the participants of the 2018 ICBEM conference for vigorous and interesting discussions.

CONFLICT OF INTEREST

The authors report no conflicts of interest.

REAGENT AVAILABILITY

The construct encoding iGlucoSnFR-TS has been deposited at Addgene (addgene.com).

AUTHOR CONTRIBUTIONS

Conceptualization, C.M.D.-G., C.L., and G.Y.; *Methodology*, C.M.D.-G., C.L., and G.Y.; *Software*, G.Y.; *Investigation*, C.M.D.-G., C.L., B.L., D.K., J.R.M.-F., N.N., and M.R.; *Formal Analysis*, C.M.D.-G., C.L., and G.Y.; *Resources*, J.S.M., J.P.K., and L.L.L.; *Writing – Original Draft*, C.M.D.-G., J.R.M.-F. and G.Y.; *Writing – Review & Editing*, C.M.D.-G., C.L., J.R.M.-F., B.L., D.K., N.N., M.R., J.S.M., J.P.K., L.L.L., and G.Y.; *Visualization*, C.M.D.-G., C.L., and G.Y.; *Supervision*, G.Y.; *Funding Acquisition*, C.M.D.-G., C.L., D.K., and G.Y.

ORCID

Carlos Manlio Díaz-García https://orcid.org/0000-0002-4352-2496
Juan Ramón Martínez-François https://orcid.org/0000-0002-1035-2574
Jonathan S. Marvin https://orcid.org/0000-0003-2294-4515
Gary Yellen https://orcid.org/0000-0003-4228-7866

REFERENCES

Alberts, B., Johnson, A., Lewis, J., Raff, M., Roberts, K., & Walter, P. (2002). Membrane transport of small molecules and the electrical properties of membranes. In *Molecular biology of the cell* (4th ed.). Retrieved from https://www.ncbi.nlm.nih.gov/books/NBK21044/

Andermann, M. L., Kerlin, A. M., & Reid, R. C. (2010). Chronic cellular imaging of mouse visual cortex during operant behavior and passive viewing. *Frontiers in Cellular Neuroscience*, *4*, 3. https://doi.org/10.3389/fncel.2010.00003

Bak, L. K., & Walls, A. B. (2018). CrossTalk opposing view: Lack of evidence supporting an astrocyte-to-neuron lactate shuttle coupling neuronal activity to glucose utilisation in the brain. *The Journal of Physiology*, *596*(3), 351–353. https://doi.org/10.1113/JP274945

Barros, L. F., & Weber, B. (2018). CrossTalk proposal: An important astrocyte-to-neuron lactate shuttle couples neuronal activity to glucose utilisation in the brain. *The Journal of Physiology*, *596*(3), 347–350. https://doi.org/10.1113/JP274944

Bittner, C. X., Loaiza, A., Ruminot, I., Larenas, V., Sotelo-Hitschfe, T., Gutiérrez, R., … Barros, L. F. (2010). High resolution measurement of the glycolytic rate. *Frontiers in Neuroenergetics*, *2*. https://doi.org/10.3389/fnene.2010.00026

Bittner, C. X., Valdebenito, R., Ruminot, I., Loaiza, A., Larenas, V., Sotelo-Hitschfeld, T., … Barros, L. F. (2011). Fast and reversible stimulation of astrocytic glycolysis by K+ and a delayed and persistent effect of glutamate. *Journal of Neuroscience*, *31*(12), 4709–4713. https://doi.org/10.1523/JNEUROSCI.5311-10.2011

Choi, I. Y., Lee, S. P., Kim, S. G., & Gruetter, R. (2001). In vivo measurements of brain glucose transport using the reversible Michaelis-Menten model and simultaneous measurements of cerebral blood flow changes during hypoglycemia. *Journal of Cerebral Blood Flow and Metabolism: Official Journal of the International Society of Cerebral Blood Flow and Metabolism*, *21*(6), 653–663. https://doi.org/10.1097/00004647-200106000-00003

Chuquet, J., Quilichini, P., Nimchinsky, E. A., & Buzsáki, G. (2010). Predominant enhancement of glucose uptake in astrocytes versus neurons during activation of the somatosensory cortex. *The Journal of Neuroscience: The Official Journal of the Society for Neuroscience*, *30*(45), 15298–15303. https://doi.org/10.1523/JNEUROSCI.0762-10.2010

Cremer, J. E., Seville, M. P., & Cunningham, V. J. (1988). Tracer 2-deoxyglucose kinetics in brain regions of rats given kainic acid. *Journal of Cerebral Blood Flow & Metabolism*, *8*(2), 244–253. https://doi.org/10.1038/jcbfm.1988.55

Cuneo, M. J., Changela, A., Warren, J. J., Beese, L. S., & Hellinga, H. W. (2006). The crystal structure of a thermophilic glucose binding protein reveals adaptations that interconvert mono and di-saccharide binding sites. *Journal of Molecular Biology*, *362*(2), 259–270. https://doi.org/10.1016/j.jmb.2006.06.084

Díaz-García, C. M., Mongeon, R., Lahmann, C., Koveal, D., Zucker, H., & Yellen, G. (2017). Neuronal stimulation triggers neuronal glycolysis and not lactate uptake. *Cell Metabolism*, *26*(2), 361–374.e4. https://doi.org/10.1016/j.cmet.2017.06.021

Dienel, G. A. (2012). Fueling and imaging brain activation. *ASN Neuro*, *4*(5). https://doi.org/10.1042/AN20120021

Dienel, G. A. (2013). Astrocytic energetics during excitatory neurotransmission: What are contributions of glutamate oxidation and glycolysis? *Neurochemistry International*, *63*(4), 244–258. https://doi.org/10.1016/j.neuint.2013.06.015

Dienel, G. A., Cruz, N. F., Mori, K., Holden, J. E., & Sokoloff, L. (1991). Direct measurement of the lambda of the lumped constant of the deoxyglucose method in rat brain: Determination of lambda and lumped constant from tissue glucose concentration or equilibrium brain/plasma distribution ratio for methylglucose. *Journal of Cerebral Blood Flow and Metabolism: Official Journal of the International Society of Cerebral Blood Flow and Metabolism*, *11*(1), 25–34. https://doi.org/10.1038/jcbfm.1991.3

Dittmer, P. J., Miranda, J. G., Gorski, J. A., & Palmer, A. E. (2009). Genetically encoded sensors to elucidate spatial distribution of cellular zinc. *Journal of Biological Chemistry*, *284*(24), 16289–16297. https://doi.org/10.1074/jbc.M900501200

Duarte, J. M. N., & Gruetter, R. (2012). Characterization of cerebral glucose dynamics in vivo with a four-state conformational model of transport at the blood–brain barrier. *Journal of Neurochemistry*, *121*(3), 396–406. https://doi.org/10.1111/j.1471-4159.2012.07688.x

Duarte, J. M. N., Morgenthaler, F. D., Lei, H., Poitry-Yamate, C., & Gruetter, R. (2009). Steady-state brain glucose transport kinetics re-evaluated with a four-state conformational model. *Frontiers in Neuroenergetics*, *1*, 6. https://doi.org/10.3389/neuro.14.006.2009

Engl, E., Jolivet, R., Hall, C. N., & Attwell, D. (2017). Non-signalling energy use in the developing rat brain. *Journal of Cerebral Blood Flow & Metabolism*, *37*(3), 951–966. https://doi.org/10.1177/0271678X16648710

Fehr, M., Lalonde, S., Ehrhardt, D. W., & Frommer, W. B. (2004). Live imaging of glucose homeostasis in nuclei of COS-7 cells. *Journal of Fluorescence*, *14*(5), 603–609. https://doi.org/10.1023/B:JOFL.0000039347.94943.99

Fox, P. T., Raichle, M. E., Mintun, M. A., & Dence, C. (1988). Nonoxidative glucose consumption during focal physiologic neural activity. *Science (New York, N.Y.)*, *241*(4864), 462–464.

Good, N. E., Winget, G. D., Winter, W., Connolly, T. N., Izawa, S., & Singh, R. M. M. (1966). Hydrogen ion buffers for biological research. *Biochemistry*, *5*(2), 467–477. https://doi.org/10.1021/bi00866a011

Grienberger, C., & Konnerth, A. (2012). Imaging calcium in neurons. *Neuron*, *73*(5), 862–885. https://doi.org/10.1016/j.neuron.2012.02.011

Habicht, G. S. (1981). Body temperature in normal and endotoxin-treated mice of different ages. *Mechanisms of Ageing and Development*, *16*(1), 97–104. https://doi.org/10.1016/0047-6374(81)90037-3

Hung, Y. P., Albeck, J. G., Tantama, M., & Yellen, G. (2011). Imaging cytosolic NADH-NAD(+) redox state with a genetically encoded fluorescent biosensor. *Cell Metabolism*, *14*(4), 545–554. https://doi.org/10.1016/j.cmet.2011.08.012

Ivanov, A., & Zilberter, Y. (2011). Critical state of energy metabolism in brain slices: The principal role of oxygen delivery and energy substrates in shaping neuronal activity. *Frontiers in Neuroenergetics*, *3*, 9. https://doi.org/10.3389/fnene.2011.00009

Jang, C., Chen, L., & Rabinowitz, J. D. (2018). Metabolomics and isotope tracing. *Cell*, *173*(4), 822–837. https://doi.org/10.1016/j.cell.2018.03.055

Keller, J. P., & Looger, L. L. (2016). The oscillating stimulus transporter assay, OSTA: Quantitative functional imaging of transporter protein activity in time and frequency domains. *Molecular Cell*, *64*(1), 199–212. https://doi.org/10.1016/j.molcel.2016.09.001

Keller, J. P., Marvin, J. S., Lacin, H., Lemon, W. C., Shea, J., Kim, S., … Looger, L. L. (2019). Glucose imaging in multiple model organisms with an engineered single-wavelength sensor. *BioRxiv*. https://doi.org/10.1101/571422

Kovacic, P. B., Chowdhury, H. H., Velebit, J., Kreft, M., Jensen, J., & Zorec, R. (2011). New insights into cytosolic glucose levels during differentiation of 3T3-L1 fibroblasts into adipocytes. *The Journal of Biological Chemistry*, *286*(15), 13370–13381. https://doi.org/10.1074/jbc.M110.200980

Lang, K., Wagner, C., Haddad, G., Burnekova, O., & Geibel, J. (2003). Intracellular pH activates membrane-bound Na(+)/H(+) exchanger and vacuolar H(+)-ATPase in human embryonic kidney (HEK) cells. *Cellular Physiology and Biochemistry: International Journal of Experimental Cellular Physiology, Biochemistry, and Pharmacology*, *13*(5), 257–262. https://doi.org/10.1159/000074540

Leen, W. G., Willemsen, M. A., Wevers, R. A., & Verbeek, M. M. (2012). Cerebrospinal fluid glucose and lactate: Age-specific reference values and implications for clinical practice. *PLoS ONE*, *7*(8), e42745. https://doi.org/10.1371/journal.pone.0042745

Lewis, L. D., Ljunggren, B., Norberg, K., & Siesjö, B. K. (1974). Changes in carbohydrate substrates, amino acids and ammonia in the brain during insulin-induced hypoglycemia. *Journal of Neurochemistry*, *23*(4), 659–671. https://doi.org/10.1111/j.1471-4159.1974.tb04389.x

Looger, L. L., Lalonde, S., & Frommer, W. B. (2005). Genetically encoded FRET sensors for visualizing metabolites with subcellular resolution in living cells. *Plant Physiology*, *138*(2), 555–557. https://doi.org/10.1104/pp.104.900151

Lundgaard, I., Li, B., Xie, L., Kang, H., Sanggaard, S., Haswell, J. D. R., … Nedergaard, M. (2015). Direct neuronal glucose uptake heralds activity-dependent increases in cerebral metabolism. *Nature Communications*, *6*, 6807. https://doi.org/10.1038/ncomms7807

Lutas, A., Birnbaumer, L., & Yellen, G. (2014). Metabolism regulates the spontaneous firing of substantia nigra pars reticulata neurons via KATP and nonselective cation channels. *The Journal of Neuroscience*, *34*(49), 16336–16347. https://doi.org/10.1523/JNEUROSCI.1357-14.2014

Lyons, D. G., Parpaleix, A., Roche, M., & Charpak, S. (2016). Mapping oxygen concentration in the awake mouse brain. *Elife*, *5*, e12024. https://doi.org/10.7554/eLife.12024

Magistretti, P. J., Sorg, O., Yu, N., Martin, J. L., & Pellerin, L. (1993). Neurotransmitters regulate energy metabolism in astrocytes: Implications for the metabolic trafficking between neural cells. *Developmental Neuroscience*, *15*(3–5), 306–312. https://doi.org/10.1159/000111349

Marvin, J. S., Looger, L., Lee, R. T., & Schreiter, E. (2018). *patent #9939437*. Retrieved from http://patft.uspto.gov/netacgi/nph-Parser?Sect1=PTO2&Sect2=HITOFF&p=1&u=%2Fnetahtml%2FPTO%2Fsearch-bool.html&r=1&f=G&l=50&co1=AND&d=PTXT&s1=9939437.PN.&OS=PN/9939437&RS=PN/9939437

Masia, R., Krause, D. S., & Yellen, G. (2015). The inward rectifier potassium channel Kir2.1 is expressed in mouse neutrophils from bone marrow and liver. *American Journal of Physiology—Cell Physiology*, *308*(3), C264–C276. https://doi.org/10.1152/ajpcell.00176.2014

Mergenthaler, P., Lindauer, U., Dienel, G. A., & Meisel, A. (2013). Sugar for the brain: The role of glucose in physiological and pathological brain function. *Trends in Neurosciences*, *36*(10), 587–597. https://doi.org/10.1016/j.tins.2013.07.001

Mongeon, R., Venkatachalam, V., & Yellen, G. (2016). Cytosolic NADH-NAD(+) redox visualized in brain slices by two-photon fluorescence lifetime biosensor imaging. *Antioxidants & Redox Signaling*, *25*(10), 553–563. https://doi.org/10.1089/ars.2015.6593

Morikawa, T. J., Fujita, H., Kitamura, A., Horio, T., Yamamoto, J., Kinjo, M., … Watanabe, T. M. (2016). Dependence of fluorescent protein brightness on protein concentration in solution and enhancement of it. *Scientific Reports*, *6*, 22342. https://doi.org/10.1038/srep22342

O'Connor, D. H., Peron, S. P., Huber, D., & Svoboda, K. (2010). Neural activity in barrel cortex underlying vibrissa-based object localization in mice. *Neuron*, *67*(6), 1048–1061. https://doi.org/10.1016/j.neuron.2010.08.026

Pfeuffer, J., Tkáč, I., & Gruetter, R. (2000). Extracellular-intracellular distribution of glucose and lactate in the rat brain assessed noninvasively by diffusion-weighted ^{1}H nuclear magnetic resonance spectroscopy *in vivo*. *Journal of Cerebral Blood Flow & Metabolism*, *20*(4), 736–746. https://doi.org/10.1097/00004647-200004000-00011

Piquet, J., Toussay, X., Hepp, R., Lerchundi, R., Le Douce, J., Faivre, É., … Cauli, B. (2018). Supragranular pyramidal cells exhibit early metabolic alterations in the 3xTg-AD mouse model of Alzheimer's disease. *Frontiers in Cellular Neuroscience*, *12*, 216. https://doi.org/10.3389/fncel.2018.00216

Pologruto, T. A., Sabatini, B. L., & Svoboda, K. (2003). ScanImage: Flexible software for operating laser scanning microscopes. *Biomedical Engineering Online*, *2*, 13. https://doi.org/10.1186/1475-925X-2-13

Porras, O. H., Loaiza, A., & Barros, L. F. (2004). Glutamate mediates acute glucose transport inhibition in hippocampal neurons. *The Journal of Neuroscience: The Official Journal of the Society for Neuroscience*, *24*(43), 9669–9673. https://doi.org/10.1523/JNEUROSCI.1882-04.2004

Prebil, M., Vardjan, N., Jensen, J., Zorec, R., & Kreft, M. (2011). Dynamic monitoring of cytosolic glucose in single astrocytes. *Glia*, *59*(6), 903–913. https://doi.org/10.1002/glia.21161

Romani, A., & Scarpa, A. (1992). Regulation of cell magnesium. *Archives of Biochemistry and Biophysics*, *298*(1), 1–12.

Ruminot, I., Schmälzle, J., Leyton, B., Barros, L. F., & Deitmer, J. W. (2019). Tight coupling of astrocyte energy metabolism to synaptic activity revealed by genetically encoded FRET nanosensors in hippocampal tissue. *Journal of Cerebral Blood Flow and Metabolism*, *39*(3), 513–523. https://doi.org/10.1177/0271678X17737012 (Epub 2017 Oct 30).

Salvi, A., Quillan, J. M., & Sadée, W. (2002). Monitoring intracellular pH changes in response to osmotic stress and membrane transport activity using 5-chloromethylfluorescein. *AAPS PharmSci*, *4*(4), E21. https://doi.org/10.1208/ps040421

Schoenmakers, T. J., Visser, G. J., Flik, G., & Theuvenet, A. P. (1992). CHELATOR: An improved method for computing metal ion concentrations in physiological solutions. *BioTechniques*, *12*(6), 870–874, 876–879.

Silver, I. A., & Erecińska, M. (1994). Extracellular glucose concentration in mammalian brain: Continuous monitoring of changes during increased neuronal activity and upon limitation in oxygen supply in normo-, hypo-, and hyperglycemic animals. *The Journal of Neuroscience: The Official Journal of the Society for Neuroscience*, *14*(8), 5068–5076.

Sokoloff, L., Reivich, M., Kennedy, C., Rosiers, M. H. D., Patlak, C. S., Pettigrew, K. D., … Shinohara, M. (1977). The [14C]deoxyglucose method for the measurement of local cerebral glucose utilization: Theory, procedure, and normal values in the conscious and anesthetized albino rat. *Journal of Neurochemistry*, *28*(5), 897–916. https://doi.org/10.1111/j.1471-4159.1977.tb10649.x

Takanaga, H., Chaudhuri, B., & Frommer, W. B. (2008). GLUT1 and GLUT9 as the major contributors to glucose influx in HEPG2 cells identified by a high sensitivity intramolecular FRET glucose sensor. *Biochimica et Biophysica Acta*, *1778*(4), 1091–1099. https://doi.org/10.1016/j.bbamem.2007.11.015

Tantama, M., Hung, Y. P., & Yellen, G. (2011). Imaging intracellular pH in live cells with a genetically encoded red fluorescent protein sensor. *Journal of the American Chemical Society*, *133*(26), 10034–10037. https://doi.org/10.1021/ja202902d

Tong, J., McCarthy, T. V., & MacLennan, D. H. (1999). Measurement of resting cytosolic Ca^{2+} concentrations and Ca^{2+} store size in HEK-293 cells transfected with malignant hyperthermia or central core disease mutant Ca^{2+} release channels. *The Journal of Biological Chemistry*, *274*(2), 693–702.

van de Ven, K. C. C., de Galan, B. E., van der Graaf, M., Shestov, A. A., Henry, P.-G., Tack, C. J. J., & Heerschap, A. (2011). Effect of acute hypoglycemia on human cerebral glucose metabolism measured by 13C magnetic resonance spectroscopy. *Diabetes*, *60*(5), 1467–1473. https://doi.org/10.2337/db10-1592

Yasuda, R., Harvey, C. D., Zhong, H., Sobczyk, A., van Aelst, L., & Svoboda, K. (2006). Supersensitive ras activation in dendrites and spines revealed by two-photon fluorescence lifetime imaging. *Nature Neuroscience*, *9*, 283–291.

Yellen, G., & Mongeon, R. (2015). Quantitative two-photon imaging of fluorescent biosensors. *Current Opinion in Chemical Biology*, *27*, 24–30. https://doi.org/10.1016/j.cbpa.2015.05.024

Zapata-Hommer, O., & Griesbeck, O. (2003). Efficiently folding and circularly permuted variants of the Sapphire mutant of GFP. *BMC Biotechnology*, *3*(1), 5. https://doi.org/10.1186/1472-6750-3-5

Zhang, L., Su, F., Buizer, S., Kong, X., Lee, F., Day, K., … Meldrum, D. R. (2014). A polymer-based ratiometric intracellular glucose sensor. *Chemical Communications (Cambridge, England)*, *50*(52), 6920–6922. https://doi.org/10.1039/c4cc01110d

SUPPORTING INFORMATION

Additional supporting information may be found online in the Supporting Information section at the end of the article.

Supplementary Figure 1 Comparison of iGlucoSnFR-TS lifetime values in neurons located at different depths within brain slices. Hippocampal neurons were imaged at four different depths, in the presence of different glucose concentrations ($[glucose]_o$) in the ACSF as indicated in the *x*-axis. The right *y*-axis indicates the calculated intracellular glucose concentration ($[glucose]_i$) using the equation derived from the in-cell calibration in permeabilized cells. Data sets contain 40–51 neurons, 4 slices, and 2 mice for $[glucose]_o$ = 0.5 mM; or 54–69 neurons, 6 slices and 3 mice for the remaining glucose concentrations tested in ACSF. The data set for depth = 200 μm consists of 85 neurons from 5 slices and 3 mice, recorded at a $[glucose]_o$ = 10 mM. In dentate granule neurons from hippocampal slices, the median $[glucose]_i$ was 15–25% of the $[glucose]_o$ for the interval 2–10 mM glucose. Significance levels were obtained using an unpaired non-parametric Kruskal–Wallis test with a Dunn's post hoc test for multiple comparisons.

Transparent Science Questionnaire for Authors.

How to cite this article: Díaz-García CM, Lahmann C, Martínez-François JR, et al. Quantitative *in vivo* imaging of neuronal glucose concentrations with a genetically encoded fluorescence lifetime sensor. *J Neuro Res*. 2019;97:946–960. https://doi.org/10.1002/jnr.24433